Density Dependence of the Momentum Distribution in Normal Liquid ^{4}He

K. W. Herwig, P. E. Sokol
Department of Physics
The Pennsylvania State University
University Park. PA 16802

T. R. Sosnick [†], W. M. Snow [‡], and R. C. Blasdell [*]
Materials Science Division and IPNS
Argonne National Laboratory
Argonne, IL 60439

Deep inelastic neutron scattering measurements on normal liquid ^{4}He at 4.25 K have been carried out at eleven densities between 0.125 (saturated vapor pressure) and 0.200 gm/cm^3, at a momentum transfer of 23 Å^{-1}. A sum of two Gaussians is required to characterize the scattering at all densities, even when the broadening due to instrumental resolution and corrections to the impulse approximation are included. The kinetic energy varies from 15.5 K at 0.125 gm/cm^3 to 32.7 K at 0.200 gm/cm^3.

PACS categories: 67.40.-w: 61.12.Gz: 61.12.Bt

[†] Present Address: Division of Biological Sciences. Los Alamos National Laboratory

[‡] Permanent Address: Lyman Laboratory of Physics, Harvard University. Cambridge. MA 02138

[*] Permanent Address: Dept. of Physics. University of Illinois at Urbana-Champaign. Urbana. IL 61801

1. INTRODUCTION

Condensed ^{4}He, as the prototypical system of interacting bosons, is of great interest to both theoreticians and experimentalists. Theoretical attempts to describe the behavior of liquid ^{4}He have been extensively compared to a host of experimental measurements in order to check the applicability of these treatments. Although much of this effort has been devoted to studies of the interesting properties of superfluid ^{4}He, the normal liquid has also been the object of a substantial amount of experimental and theoretical work.

There are currently no comprehensive analytic theories capable of determining the momentum distribution of condensed helium. Computer simulations seem to present the most realistic description of condensed helium, but until recently, most of these[1,2] considered only the ground state or low excited state properties. In contrast, Path Integral Monte Carlo (PIMC) methods have been very successful in calculating the properties of both normal liquid and superfluid helium over a wide range of temperatures and densities.[3] Measurements of the density dependence of the momentum distribution and the kinetic energy in the normal liquid provide a valuable and unique test for these difficult calculations.

The momentum distribution of liquid helium can in principle be determined from inelastic neutron scattering measurements at high momentum transfers, Q, using the Impulse Approximation[4] (IA). Several previous measurements have studied the inelastic scattering from the normal fluid at saturated vapor pressure.[5-14] Reported values of the single particle kinetic energies, which can be obtained directly from the second moment of the scattering (regardless of the validity of the IA), range from 13.6 to 16.9 K at 4.25 K and a density of 0.125 gm/cc. Additionally, the momentum distribution in the normal liquid has been reported as Gaussian over three orders of magnitude.

In this paper we report deep inelastic scattering measurements of normal liquid ^{4}He at 4.25 K at eleven densities ranging from 0.125 to 0.200 gm/cm^3. Our measurements are at sufficiently high Q, approximately 23 Å^{-1}, that deviations from the IA are small and may be taken into account using a recent theoretical treatment by Silver.[15,16] We find that the kinetic energy increases in a monotonic fashion with density and is quite comparable to the PIMC results. The data are also consistent with the momentum distribution generated by the PIMC calculation.

1

Density Dependence of the Momentum Distribution in Normal Liquid ^{4}He

K. W. Herwig, P. E. Sokol

Department of Physics

The Pennsylvania State University

University Park, PA 16802

T. R. Sosnick [†], W. M. Snow [‡], and R. C. Blasdell [*]

Materials Science Division and IPNS

Argonne National Laboratory

Argonne, IL 60439

Deep inelastic neutron scattering measurements on normal liquid ^{4}He at 4.25 K have been carried out at eleven densities between 0.125 (saturated vapor pressure) and 0.200 gm/cm^3, at a momentum transfer of 23 Å^{-1}. A sum of two Gaussians is required to characterize the scattering at all densities, even when the broadening due to instrumental resolution and corrections to the impulse approximation are included. The kinetic energy varies from 15.5 K at 0.125 gm/cm^3 to 32.7 K at 0.200 gm/cm^3.

PACS categories: 67.40.-w; 61.12.Gz; 61.12.Bt

[†] Present Address: Division of Biological Sciences, Los Alamos National Laboratory

[‡] Permanent Address: Lyman Laboratory of Physics, Harvard University, Cambridge, MA 02138

[*] Permanent Address: Dept. of Physics, University of Illinois at Urbana-Champaign, Urbana, IL 61801

1. INTRODUCTION

Condensed ^{4}He, as the prototypical system of interacting bosons, is of great interest to both theoreticians and experimentalists. Theoretical attempts to describe the behavior of liquid ^{4}He have been extensively compared to a host of experimental measurements in order to check the applicability of these treatments. Although much of this effort has been devoted to studies of the interesting properties of superfluid ^{4}He, the normal liquid has also been the object of a substantial amount of experimental and theoretical work.

There are currently no comprehensive analytic theories capable of determining the momentum distribution of condensed helium. Computer simulations seem to present the most realistic description of condensed helium, but until recently, most of these[1,2] considered only the ground state or low excited state properties. In contrast, Path Integral Monte Carlo (PIMC) methods have been very successful in calculating the properties of both normal liquid and superfluid helium over a wide range of temperatures and densities.[3] Measurements of the density dependence of the momentum distribution and the kinetic energy in the normal liquid provide a valuable and unique test for these difficult calculations.

The momentum distribution of liquid helium can in principle be determined from inelastic neutron scattering measurements at high momentum transfers, Q, using the Impulse Approximation[4] (IA). Several previous measurements have studied the inelastic scattering from the normal fluid at saturated vapor pressure.[5−14] Reported values of the single particle kinetic energies, which can be obtained directly from the second moment of the scattering (regardless of the validity of the IA), range from 13.6 to 16.9 K at 4.25 K and a density of 0.125 gm/cc. Additionally, the momentum distribution in the normal liquid has been reported as Gaussian over three orders of magnitude.

In this paper we report deep inelastic scattering measurements of normal liquid ^{4}He at 4.25 K at eleven densities ranging from 0.125 to 0.200 gm/cm^3. Our measurements are at sufficiently high Q, approximately 23 Å^{-1}, that deviations from the IA are small and may be taken into account using a recent theoretical treatment by Silver.[15,16] We find that the kinetic energy increases in a monotonic fashion with density and is quite comparable to the PIMC results. The data are also consistent with the momentum distribution generated by the PIMC calculation.

i

2. DEEP INELASTIC NEUTRON SCATTERING

The scattering of neutrons by helium is described by the double-differential cross-section

$$\frac{d^2\sigma}{d\Omega d\omega} = b^2 \frac{k_f}{k_i} S(Q,\omega) \qquad (2.1)$$

where b is the bound scattering length of helium, k_i and k_f are respectively the initial and final momentum of the neutron, and Q and ω are the momentum and energy transfer respectively. The dynamic structure factor $S(Q,\omega)$ describes the dynamics of the helium sample.

In the limit that $Q/2\pi$ is large compared with the nearest neighbor distance (for helium[17] this implies Q greater than or on the order of 10 Å^{-1}) the incoherent approximation holds and we can write

$$S_{inc}(Q,\omega) = \int_{-\infty}^{+\infty} \exp(-\frac{i\omega t}{\hbar}) < \exp[-i\vec{Q}\cdot\vec{r}(0)]\exp[-i\vec{Q}\cdot\vec{r}(t)] > dt \qquad (2.2)$$

where $\vec{r}(t)$ is the position vector of an atom and $< ... >$ signifies a thermodynamic average. In the incoherent approximation interference effects due to correlations between the atoms average out, and the scattering from each atom can be treated independently. Moments of this function can be derived and in particular the second moment may be written as[18]

$$M_2(Q) = \int (\omega - \omega_r)^2 S_{inc}(Q,\omega)d\omega = \frac{4}{3}\omega_r < KE > \qquad (2.3)$$

where the recoil energy, ω_r, is $\hbar^2 Q^2/2M_{He}$ and M_{He} is the mass of the recoiling atom. Under the conditions of the incoherent approximation, the average kinetic energy per atom can be obtained directly from the second moment of the observed scattering. In our experiments, Q at the center of the recoil peak is 23 Å^{-1}, and the incoherent approximation is certainly applicable.

At high momentum transfers, the form for $S(Q,\omega)$ simplifies considerably from Equation (2.2). In this limit, the impulse imparted to the target atom by the neutron during the collision far exceeds the impulse transferred by neighboring helium atoms and only single particle properties are probed. The scattering can then be described by the well known impulse approximation (IA) which directly relates $S(Q,\omega)$ to the atomic momentum distribution, $n(|\vec{p}|)$

$$\lim_{Q\to\infty} S(Q,\omega) = S_{IA}(Q,\omega) = \int_{-\infty}^{\infty} n(|\vec{p}|) \ \delta(\omega - \omega_r - \frac{\hbar\vec{Q}\cdot\vec{p}}{M_{He}})d\vec{p} \qquad (2.4)$$

2

The delta function represents the conservation of energy and momentum. In the IA the duration of the scattering event can be viewed as much shorter than the helium-helium interaction time. The recoiling atom then acts as a free-particle during the collision.

The scattering from an isotropic system, such as liquid helium, can be expressed as a function of a single scaling variable $Y \equiv (M/Q)(\omega - \omega_r)$ when the impulse approximation is obeyed.[19] The scattering, as a function of this scaling variable, may be written as

$$S_{IA}(Q,\omega) = \frac{M}{Q} J(Y) \tag{2.5}$$

where $J(Y)$ is readily interpreted as the longitudinal momentum distribution and Y as the z component of the momentum

$$J(Y) = \int_{-\infty}^{\infty} \int_{-\infty}^{\infty} dp_x \; dp_y \; n(p_x, p_y, Y) \tag{2.6}$$

In the IA, $J(Y)$ depends only on Y and is symmetric about $Y = 0$. This behavior of $J(Y)$ is just the Y-space manifestation of the well known characteristics of the IA, that the scattering function is centered at the recoil energy and, at constant Q, is symmetric with a width proportional to Q.

The IA only approximately describes the scattering for currently accessible momentum transfers. Deviations from the IA, known as final state effects (FSE), result from the interaction of the recoiling helium atom with its neighbors during the scattering process. These interactions alter the ideal free-particle behavior of the final state of the recoiling atom required for the validity of the IA. At high Q's the observed scattering approximately scales[20] with Y and final state effects, while certainly present, are amenable to theoretical treatment.

In the analysis of our data, we make use of a theory by Silver[15,16] which expresses FSE as a convolution with the IA result

$$J(Y) = \int_{-\infty}^{+\infty} R(Y - Y') J_{IA}(Y') dY' \tag{2.7}$$

where $R(Y)$ is the final state broadening. This broadening, which depends only on the measured pair correlation function and interatomic potential, varies slowly with Q and has been approximated as a function of Y only. The shape of the final state broadening is shown in Figure 1. The negative tails in $R(Y)$ are necessary since the scattering must obey the second moment sum rule for incoherent scattering (Equation (2.3)) requiring $R(Y)$ to

3

have zero second moment. We note that FSE have little effect on the broad scattering observed in the normal liquid and that we take them into account only for completeness. Several other procedures, or ignoring FSE altogether, would give similar results.

The final state broadening may be viewed[15,16] as the Fourier transform of the probability that the recoiling atom will not collide with a neighboring atom as a function of distance and is thus dependent on the density. In Silver's theory, this probability depends on the interatomic potential and pair correlation function, $g(r)$, only the latter of which is density dependent. Since, to a first approximation, $g(r)$ scales with the density, $R(Y)$ will also scale with the density.[21] The final state broadening at a density ρ_2 may be obtained from the broadening at a different density ρ_1 by

$$R_2(Y) = R_1 \left(\frac{\rho_2}{\rho_1} Y \right) \tag{2.8}$$

where $R_1(Y)$ and $R_2(Y)$ are the broadening at the densities ρ_1 and ρ_2 respectively. We use the final state broadening calculated by Silver [21] at a density of 0.147 gm/cm^3 and scale this result to our experimental densities using Equation (2.8).

We can obtain $n(p)$ directly from $J(Y)$ using

$$n(Y) = \frac{-1}{2\pi Y} \frac{dJ(Y)}{dY} \tag{2.9}$$

but in practice converting from an experimentally determined $J(Y)$ to $n(p)$ presents several difficulties. First, in order to use Equation (2.9) the instrumental resolution and final state effect broadening must be removed. Deconvolution, particularly on data with statistical noise, is an unstable and ill-defined procedure. Second, numerical differentiation substantially increases the error associated with the data and can only be avoided if the data is smoothed or the results are otherwise biased. Finally, in order to obtain $n(p)$ the differentiated data must be divided by Y and the results are particularly susceptible to any statistical fluctuations at small Y. In this paper we limit our analysis to $J(Y)$ which is directly related to the experimental data and avoid all of the above problems.

3. EXPERIMENTAL DETAILS

The measurements were carried out using the PHOENIX spectrometer at the Intense Pulsed Neutron Source (IPNS) at Argonne National Laboratory. IPNS is a spallation neutron source that generates a short burst of neutrons with a usable flux over a wide range of

4

energies. PHOENIX, a high resolution time-of-flight (TOF) inelastic spectrometer, uses a mechanical Fermi chopper to select the incident energy. Low efficiency monitors placed in the neutron beam are used to measure the incident energy and to determine the parameters describing the incident pulse of neutrons. The chopper phasing for these measurements was chosen such that neutrons with a nominal incident energy of 495 meV were selected. Scattered neutrons are detected in a single high angle detector bank containing 25 equally spaced detectors with scattering angles between 135° and 145°. The detectors are approximately 3.8 m from the sample position. This choice of incident energy and scattering angle corresponds to an average momentum transfer of 23 Å^{-1} at the recoil peak of the helium sample, with a variation in Q across the detector bank of 2 Å^{-1}. A more complete description of the instrument and its use in measuring properties of condensed helium is presented elsewhere.[22]

The helium sample was contained in a cylindrical cell of 6061-T6 aluminum 0.10 m high with an inner diameter of 0.04 m and a wall thickness of 1.6 mm. The cell was attached to either the mixing chamber of a ^3He-^4He dilution refrigerator or a ^4He pot. The temperature, which was monitored using vapor pressure thermometry and germanium resistance thermometers attached to the bottom of the cell, was maintained at 4.25 ±0.05K. Data on the earlier samples was taken for about 30 hours and resulted in approximately 90,000 total integrated counts in the helium peak. Due to an increase in flux at IPNS, later samples required only about 18 hours of data collection to generate the same number of integrated counts. The scattering from liquid helium was measured at densities of 0.125, 0.130, 0.140, 0.149, 0.160, 0.173, 0.181, 0.186, 0.195, and 0.200 gm/cm^3, corresponding to pressures between SVP and 1500 PSIA. A background run of the empty sample cell was taken at the same temperature and incident neutron energy.

The integrated counts in the first beam monitor were used to normalize the flux on the sample from run to run. Both monitor spectra, which are asymmetric due largely to the moderator pulse spectrum, were fit to the results of a numerical simulation to determine the energy of the neutrons in the incident beam and the mean time of arrival at the sample. Standard techniques were used to convert the TOF data from each detector to $S(Q,\omega)$ and then to $J(Y)$. Data from the individual detectors were added together in $J(Y)$ in order to reduce the statistical uncertainty.

An accurate determination of the scattering function requires that instrumental resolution be taken into account. In general, the instrumental broadening is a complicated

function depending on both the energy and the momentum transfer.[23] In the case of helium, where the scattering is only significant near $Y = 0$, the instrumental resolution may be expressed as a simple one dimensional convolution. A Monte Carlo simulation of the instrument response is used to evaluate the instrumental broadening,[22] which is shown in Figure 1. The instrumental resolution has a FWHM of ~ 0.6 Å^{-1} and is much narrower than the total observed scattering.

An absolute intensity scale for the scattering was obtained from an experiment using a known scatterer, low density (0.0073 gm/cm^3) helium gas at 5.6 K. At this low density, only single helium scattering events are observed; multiple scattering and sample self shielding are negligible. The integrated scattering is defined to have unit area, as required by the zeroth moment sum rule. This provides an absolute intensity scale to within the 5% accuracy to which the area of the helium peak can be determined.

4. RESULTS

The observed scattering, normalized to constant incident flux and converted to $J(Y)$, for our 0.138 gm/cc sample (with the empty cell subtracted) is shown in Figure 1. The instrumental resolution and the broadening due to final state effects are also shown in Figure 1. The widths of both sources of broadening are quite comparable to each other but much less than the total width of the scattering due to the helium.

After subtraction of the empty cell signal, a small, broad sample dependent component approximately five times as wide as the helium peak, is still present. We believe this component is due to multiple scattering involving scattering initially by the liquid sample followed by scattering from the refrigerator, radiation shields, outer vacuum can, and other components of the cryostat before being detected. Similar backgrounds have been observed in other inelastic scattering experiments using the chopper spectrometers at IPNS.[22] The observed background, which depends on the sample, has been observed to be nearly independent of angle for scattering angles from 15 to 110 degrees.[22] Improved shielding of the sample cell from the cryostat used in some of the latter measurements .eported here, substantially reduced this background, verifying our identification of this additional scattering. We fit this background to a quadratic polynomial from $Y = -9$ to -6 Å^{-1} and $Y = 6$ to 9 Å^{-1}. Removing this broad component, as part of our background, does not change the shape of the observed peak within the experimental errors.

The contribution of helium-helium multiple scattering to the observed scattering from the bulk liquid was calculated using the same Monte Carlo simulation as used to generate the resolution broadened scattering. At these high Q's the multiple scattering is primarily due to low Q coherent scattering by the liquid and provides a negligible contribution to the observed scattering particularly at the lower densities.

As mentioned earlier, the second moment of the observed scattering, corrected for instrumental resolution, can be related to $< KE >$ in the incoherent approximation, regardless of final state effects. An interesting way to observe the contributions to the second moment and its associated uncertainty is to evaluate the second moment as a function of integration range

$$m_2(Y_c) = \int_{-Y_c}^{+Y_c} J(Y) Y^2 dY \tag{4.1}$$

The limiting value of m_2 provides a model independent method of determining $< KE >$ from our data. Figure 2 demonstrates the above calculation for a variety of densities. The broad background mentioned earlier was subtracted from the observed $J(Y)$ before performing the integration. The error bars shown in the plots are determined by evaluating Equation (4.1) at the minimum and maximum $J(Y)$ consistent with the uncertainty in the data. In order to determine $< KE >$ from the plots in Figure 2, the instrumental resolution broadening must be included. If the instrumental resolution function and the underlying $J(Y)$ are approximated by Gaussians, their widths add in quadrature. The second moment of the underlying $J(Y)$ can be obtained by subtracting the square of the effective Gaussian resolution second moment, ≈ 0.06 Å^{-2}, from the limiting values of m_2 shown in the plots of Figure 2. Using this method, we obtain values for $< KE >$ of 15.3 ±1.5, 17.1 ±2.1, 25.3 ±2.5, and 34.9 ±3.5 K for the samples at densities of 0.125, 0.140, 0.173, and 0.200 gm/cc respectively. It is important to note that the large errors in determining the kinetic energy result from the sensitivity of the second moment to the behavior of the scattering at large Y, and not from poor statistics in the data. The statistics of our data are quite good with a total of 90,000 counts in the helium peak and approximately 1000 counts per 0.075 Å^{-1} wide channel at the peak. The difficulty in determining the tails dominate the errors in the second moment as demonstrated in Figure 2.

We attempted to characterize the underlying momentum distribution implicit in our data by fitting the observed $J(Y)$ with a Gaussian model, implying a Gaussian $n(p)$. A Gaussian momentum distribution has been reported in previous measurements for a

7

sample at SVP.[6] The model $J(Y)$, convoluted with final state effects and the instrumental resolution, was fit to the data over various ranges of Y, but the quality of the fits was poor. A single Gaussian $J(Y)$ does not well represent the observed scattering which is consistent with the 0 K calculations of Whitlock and Panoff[1] and the finite temperature calculations of Ceperley and Pollock.[3]

In an attempt to fit the data with a more flexible model, we have used a $J(Y)$ consisting of a sum of two Gaussians (corresponding to a sum of two Gaussians in $n(p)$) with their centers constrained to the same value

$$J_{model}(Y) = \frac{A_1}{(2\pi\sigma_1^2)^{\frac{1}{2}}} \exp(-\frac{(Y - Y_{center})^2}{2\sigma_1^2}) + \frac{A_2}{(2\pi\sigma_2^2)^{\frac{1}{2}}} \exp(-\frac{(Y - Y_{center})^2}{2\sigma_2^2}) \quad (4.2)$$

The center of the Gaussians was allowed to differ from $Y = 0$ within the experimental uncertainty in determining the Y scale. We find that this model gives significantly better fits at all densities than did the single Gaussian model $J(Y)$. Figure 3 shows the two Gaussian fits to the data at four representative densities. In general, the agreement between the fits and the data is excellent. Table 1 lists the amplitudes and widths from the fits for all the densities. The particular values of these parameters quoted for a given density are only representative of an entire family of values which can equally well characterize the data because the widths and amplitudes of the fitted Gaussians are highly correlated. The model $J(Y)$ from any particular fit is indistinguishable from any other fit to the data for a given density.

The average kinetic energy per particle was determined from the two Gaussian fits and are shown in Figure 4. Table 2 lists the determined values of $< KE >$ and the associated uncertainties for all the densities. Figure 5 shows the 0.138 gm/cc data and the model $J(Y)$ (convoluted with the instrumental resolution and final state effect broadening) giving the quoted kinetic energy, 16.1 K. Also shown are the $J(Y)$ having associated kinetic energies of 14.5 and 17.7 K representing the quoted uncertainty in $< KE >$. The values for $< KE >$ and the associated uncertainties are consistent with those determined directly from the second moment of the scattering as given above. We can apply Equation (4.1) to our fitted two Gaussian model for $J(Y)$ and calculate the second moment as a function of the range of integration. Figure 6 shows the results for the same densities as plotted in Figure 2. We note the consistent behavior between Figures 2 and 6, namely a rapid rise in the second moment reaching a limiting value at Yc of about 3.2 Å^{-1} and 5.4 Å^{-1} for densities of 0.125 to 0.200 gm/cc respectively.

8

Equation (4.1) provides an interesting way to compare theoretical predictions with our fits. We calculate the second moments from $J(Y)$ determined by Ceperley[3] for several densities using the PIMC method and compare them to those determined from fits to our data. From the comparisons in Figure 7 we note a general tendency of our fitted model $J(Y)$ to increase m_2 at a slower initial rate than that determined from Ceperley's $J(Y)$. This indicates that our model $J(Y)$ have somewhat less intensity at low Y (0 to 2 Å^{-1}) but somewhat greater intensity at intermediate to high Y (3 to 4 Å^{-1}) than the theoretical $J(Y)$.

Several numerical calculations[1] of the momentum distribution have reported non-Gaussian behavior in the tails of $n(p)$. More recently, PIMC calculations[3] in the normal liquid have also indicated non-Gaussian behavior in the tails. To examine the sensitivity of our model to the tails of our data, we modify the behavior of our two Gaussian model in the low intensity region. We replace the model $n(p)$ with a sum of two Gaussians over the central region of the peak, but matched to an exponential in the tails and examined the effect on the 0.138 gm/cc data. Gaussian and exponential portions are matched at approximately 20% of the peak height, which occurs at $Y \approx 1.6$ Å^{-1}, with the constraint that the model is continuous. The width of both components were allowed to vary, subject to the constraint that the total area remained within the 5% uncertainty of the intensity calibration. The best fit obtained was almost equivalent to the best two Gaussian fit and gave a value of 16.9 K for the kinetic energy, 0.8 K greater than obtained from the two Gaussian fit. When the exponential was constrained so as to be consistent with the minimum and maximum uncertainty in the data, the kinetic energies varied from +15% to -10% of the value obtained from the original two Gaussian model. These variations are comparable to the variation in $< KE >$ obtained directly from the second moment and again indicate the difficulty in obtaining accurate information on the shape of the tails or on $< KE >$. Figure 8 shows the difference between $n(p)$ as determined by our best two Gaussian fit and the model using exponential tails. The model with exponential tails distributes more intensity to the high p region of $n(p)$ than does the simpler two Gaussian model. Both of these model $n(p)$ are consistent with our data.

5. DISCUSSION

Previous inelastic scattering measurements at SVP have generally extracted a single Gaussian momentum distribution.[5,6] Corrections for FSE were either made using approximate methods[6] or not at all.[5] Earlier inelastic scattering measurements at SVP have also

determined values for the kinetic energy which are in good agreement with our results. Harling and Gibbs,[5] using a Gaussian form and including a term to correct for FSE, obtain values of 16.3 and 15.7 ± 0.5 K at 4.19 and 4.2 K, respectively. Mook[11] obtained 16.9 K, from the second moment of $n(p)$ obtained from $S(Q, \omega)$ at a Q of 15 Å^{-1}. He observed excess scattering at $p = 2.25$ Å^{-1} which has not been observed in subsequent experiments that would tend to raise his estimate of the kinetic energy. Woods and Sears[6] obtained 13.6 K, also calculated from the second moment of $n(p)$ based on data taken at momentum transfers between 6 and 8 Å^{-1}. Our measured value of $< KE >$ at SVP of 15.5 ± 1.6 K is in reasonable agreement with these earlier results.

From Figure 4 we note the good agreement of the kinetic energy values determined from our data and those reported by Ceperley using PIMC methods. The best model $J(Y)$ determined by our data tend to have slightly less intensity at low to intermediate Y and slightly more intensity at intermediate to high Y than do the $J(Y)$ given by Ceperley as evidenced in Figure 7. This effect, however, is within the uncertainty in determining $J(Y)$ from our data. Figure 9 shows Ceperley's $J(Y)$ (convoluted with the instrumental final state effects broadening) compared with our data at nearly the same densities. We note the excellent agreement over most of the range in Y.

6. CONCLUSION

We have carried out Deep Inelastic Neutron Scattering measurements in the normal liquid phase at eleven densities from 0.130 to 0.200 gm/cc. The observed scattering is well described by the Impulse Approximation at the momentum transfers used in this experiment. The observed scattering is not well characterized by a single Gaussian, and a sum of two Gaussians was used to model the underlying $J(Y)$ indicating non-Gaussian behavior in $n(p)$. Behavior at large Y is difficult to deduce due to the low statistics in the tails of the scattering, and the data is consistent with non-Gaussian behavior at high Y, such as exponential tails in $n(p)$. We note, however, that the underlying $n(p)$ for the case of exponential tails differs little from the two Gaussian model over a large range of p (Figure 8).

The average kinetic energy per particle determined directly from the second moment of the scattering (corrected for instrumental resolution) is in good agreement with that determined from fitting the data with a sum of two Gaussians. These values are also in good agreement with the theoretical values determined by PIMC methods. The ability of

10

PIMC to calculate properties of normal liquid ^{4}He over this range of densities and at finite temperatures is remarkable. The excellent agreement between $J(Y)$ determined by PIMC methods and our data lends support to the application of PIMC to the more challenging task of calculating the momentum distribution and condensate fraction of superfluid ^{4}He.[24]

7. ACKNOWLEDGEMENTS

References

1   P. A. Whitlock and R. Panoff, Can. J. Phys. 65, 1409 (1987).

2   E. Manousakis, V. R. Pandharipande, Q. N. Usmani, Physical Review B31, 7022 (1985); E. Manousakis, V. R. Pandharipande, *ibid* ., 7029.

3   D. M. Ceperley and E. L. Pollock, Phys. Rev. Lett. 56, 351 (1986), private communication.

4   P. C. Hohenberg and P. M. Platzman, Phys. Rev. 152, 198 (1966).

5   O. K. Harling, Phys. Rev. A 3, 1073, (1971), A. G. Gibbs and O. K. Harling, *ibid*. 7, 1748, (1973).

6   A. D. B. Woods and V. F. Sears, Phys. Rev. Lett. 39, 415 (1977).

7   P. Martel, E. C. Svensson, A. D. B. Woods, V. F. Sears, and R. A. Cowley, J. Low Temp. Phys. 23, 285 (1976).

8   R. A. Cowley and A. D. B. Woods, Phys. Rev. Lett. 21, 787 (1968).

9   R. A. Cowley and A. D. B. Woods, Can. J. Phys. 49, 177 (1971).

10 V. F. Sears, E. C. Svensson, P. Martel and A. D. B. Woods, Phys. Rev. Lett. 49, 279 (1982).

11 H. A. Mook, Phys. Rev. Lett. 32, 1167 (1974).

12 H. A. Mook, Phys. Rev. Lett. 51, 1454 (1983).

13 S. Ikeda and N. Watanabe, Phys. Lett. A 121, 34 (1987).

14 R. M. Brugger, A. D. Taylor, C. E. Olsen, J. A. Goldstone, and A. K. Soper, Nucl. Instrum. Methods 221, 393 (1984).

15 R. N. Silver, Phys. Rev. B 38, 2283 (1988).

16 R. N. Silver, Phys. Rev. B 39, 4022 (1989).

17 H. R. Glyde and E. C. Svensson, Chapter 13 in *Methods of Experimental Physics* edited by D. L. Price and K. Sköld (Academic, New York 1987), Vol. 23, p. 303.

18 A. Rahman, K. S. Singwi, and A. Sjölander , Phys. Rev. 126 986 (1962).

19 V. F. Sears, Phys. Rev. B 30, 44 (1984).

20 P.E. Sokol, Can. J. Phys. 65, 1393 (1987).

21 R.N. Silver, private communication.

22 P. E. Sokol, K. W. Herwig, T. R. Sosnick, W. M. Snow, R. C. Blasdell, J. M. Carpenter, D. L. Price, G. Ostrowski, and R. Kleb, to be published.

23 C. -K. Loong, S. Ikeda, and J. M. Carpenter, Nuc. Instr. and Meth. A260, 381 (1987).

24 T. R. Sosnick, W. M. Snow, and P. E. Sokol, to be published.

ρ (gm/cc)	A_1	σ_1 (Å^{-1})	A_2	σ_2 (Å^{-1})
0.125	0.924	0.84	0.076	1.63
0.130	0.700	1.02	0.300	0.60
0.138	0.580	1.08	0.420	0.70
0.140	0.527	1.14	0.473	0.74
0.147	0.461	1.29	0.539	0.76
0.160	0.774	1.11	0.226	0.69
0.173	0.772	1.20	0.228	0.66
0.181	0.397	1.54	0.603	0.94
0.186	0.648	1.36	0.352	0.86
0.195	0.596	1.52	0.404	0.95
0.200	0.396	1.67	0.604	1.07

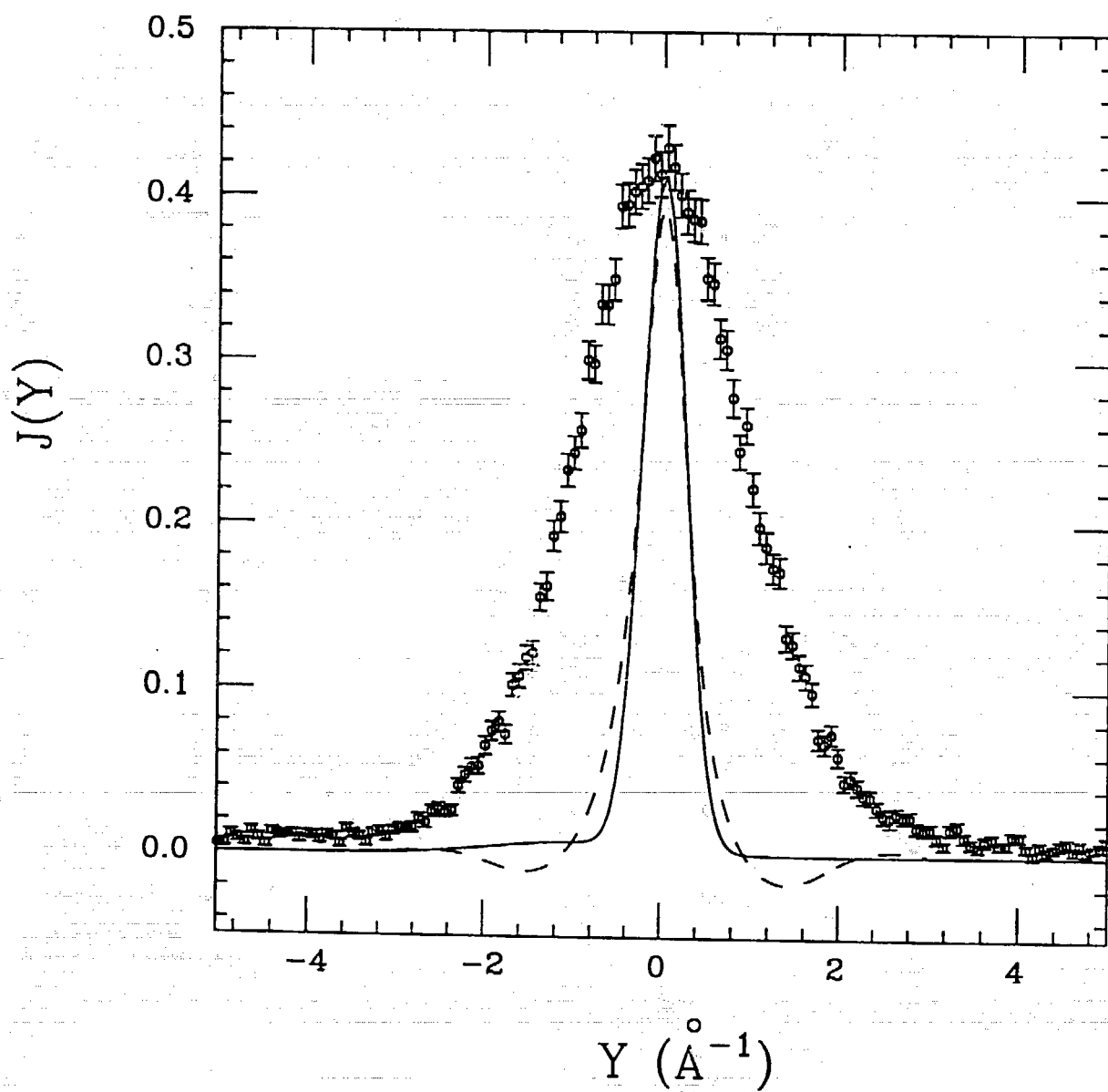Table 1: Fitted Gaussian parameters of $J(Y)$ for normal liquid ^4He.

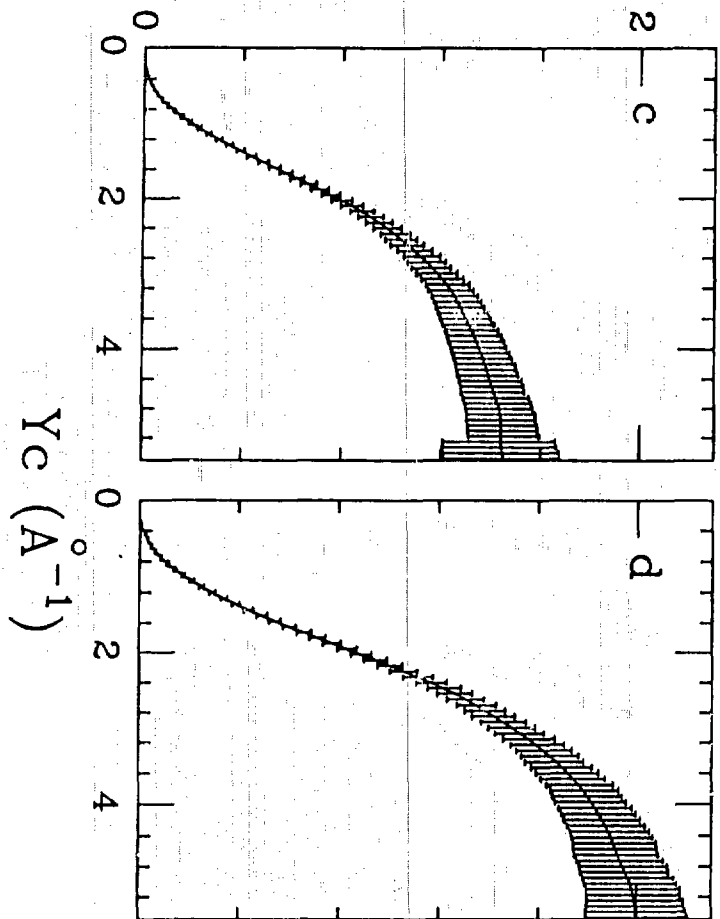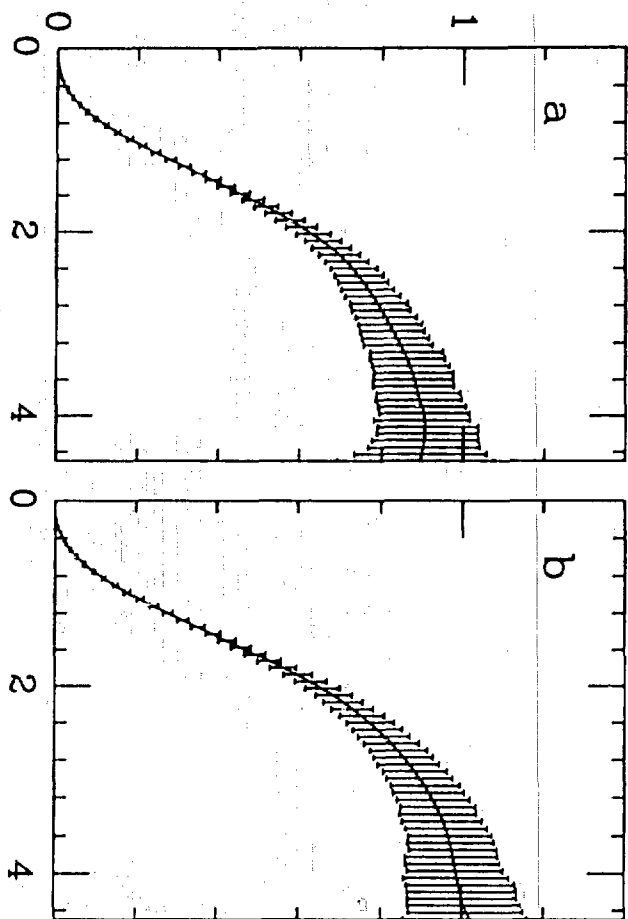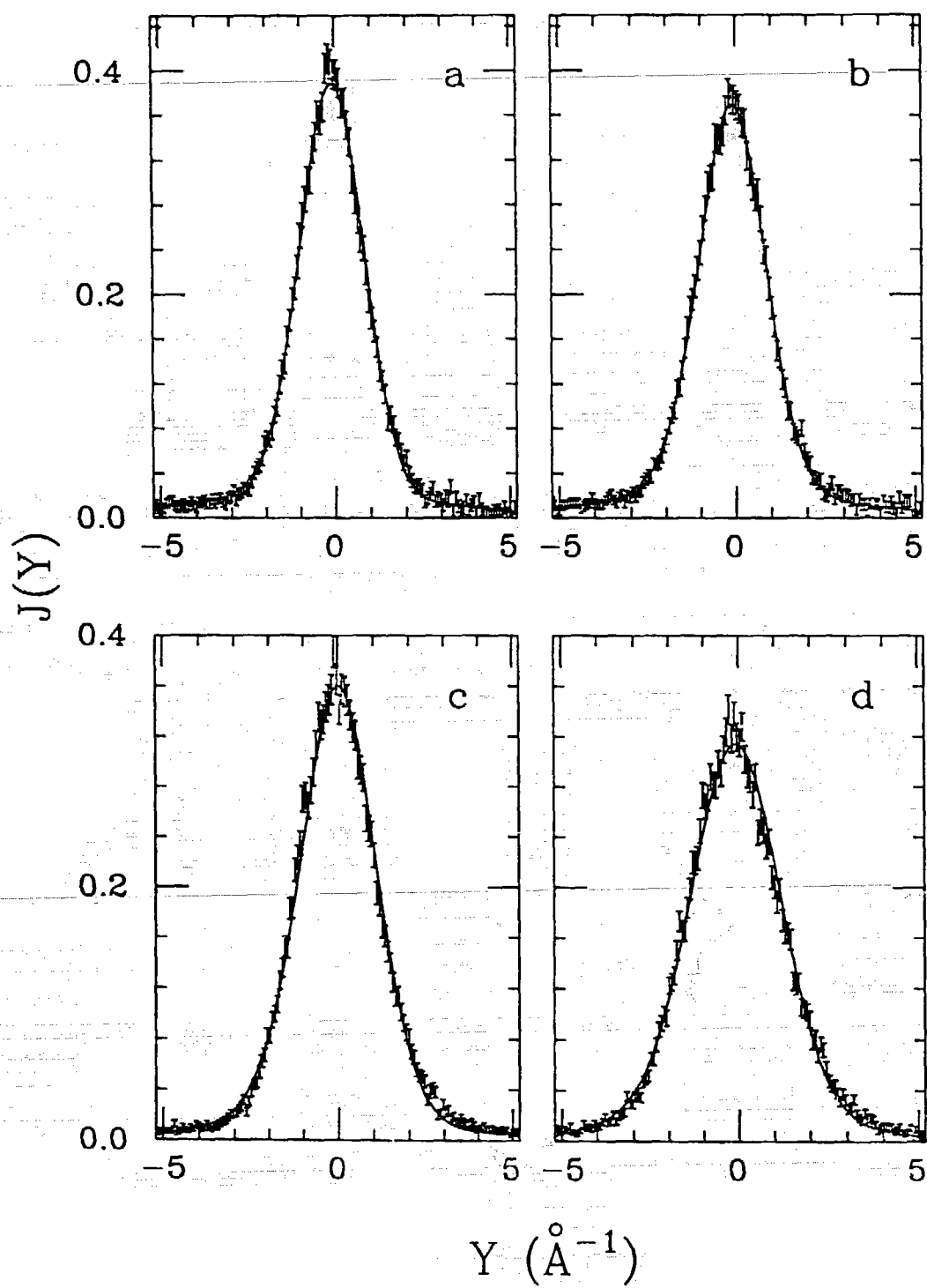| ρ (gm/cc)	$< KE >$ (K)	$\Delta < KE >$ (K)
0.125	15.5	1.6
0.130	15.2	1.5
0.138	16.1	1.6
0.140	17.1	1.7
0.147	19.6	2.0
0.160	19.2	1.9
0.173	21.8	2.2
0.181	26.5	2.7
0.186	26.5	2.7
0.195	31.6	3.2
0.200	32.7	3.3

Table 2: Single particle kinetic energies for normal liquid ^{4}He.

Figure Captions
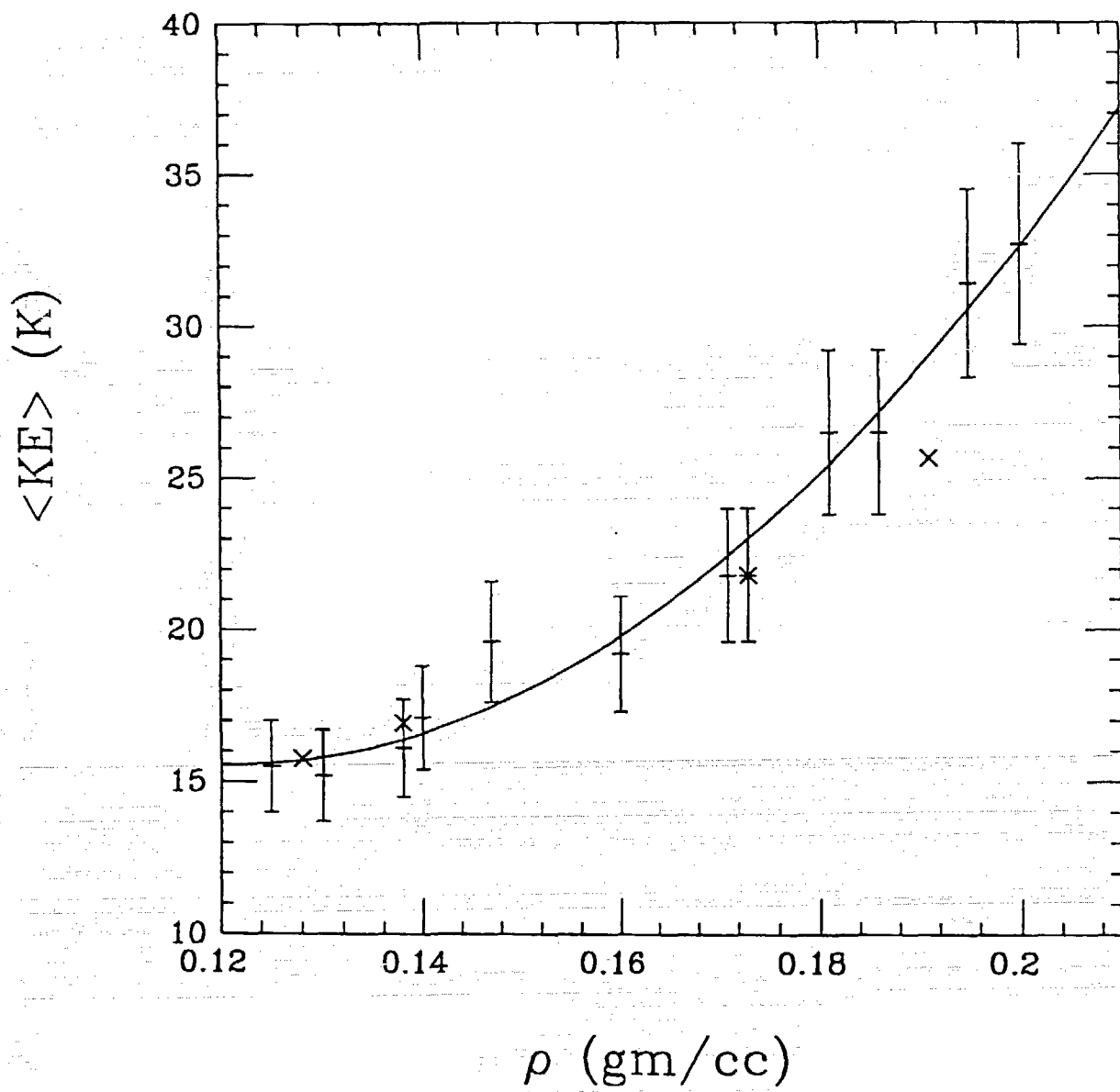
Fig. 1: Comparison of instrumental resolution (solid line), FSE (dashed line) and data at 0.138 gm/cm^3.

Fig. 2: The second moment of the experimentally determined $J(Y)$ as a function of integrating range for a variety of densities. Plots a, b, c, and d are for densities of 0.125, 0.140, 0.173, and 0.200 gm/cc respectively.

Fig. 3: Measured $J(Y)$ and two Gaussian fits for a variety of densities. The model $J(Y)$ has been broadened by the instrumental resolution and FSE. Plots a, b, c, and d are for densities of 0.125, 0.140, 0.173, and 0.200 gm/cc respectively.

Fig. 4: The measured average kinetic energy per atom as a function of density. The $\times$ are the theoretical values from Ceperley.[3] The smooth curve is from a quadratic fit to the measured points and is intended as a guide to the eye.

Fig. 5: Measured $J(Y)$ and two Gaussian fits for liquid helium at a density of 0.138 gm/cc. The three smooth curves are the model $J(Y)$ having the indicated kinetic energies.

Fig. 6: The second moment of the fitted model $J(Y)$ a function of integrating range for the indicated densities.

Fig. 7: Comparison of the second moments of $J(Y)$ determined as a function of integrating range from our fitted model and the theoretically determined $J(Y)$ from PIMC calculations.[3] The densities used in the experiment are 0.138, 0.173, and 0.186 gm/cc for plots a, b, and c respectively. The densities used in the theoretical calculation are 0.138, 0.173, and 0.191 gm/cc for plots a, b, and c respectively.

Fig. 8: $n(p)$ as determined from fits to the measured $J(Y)$ of liquid helium at a density of 0.138 gm/cc. The solid curve is the best two Gaussian fit to the data. The dashed curve is the best fit using Gaussians to model the central portion of the peak adding exponential behaviour in $n(p)$ at $Y = \pm 1.6$ Å^{-1}.

Fig. 9: Comparison of the measured and theoretical $J(Y)$. The solid curves are the theoretical $J(Y)$ from Ceperley[3] convoluted with instrumental resolution and FSE broadening. The measured $J(Y)$ are from densities of 0.138, 0.173, 0.186 gm/cc for plots a, b, and c respectively. The theoretical $J(Y)$ were calculated at densities of 0.138, 0.173, and 0.191 gm/cc for plots a, b, and c respectively.

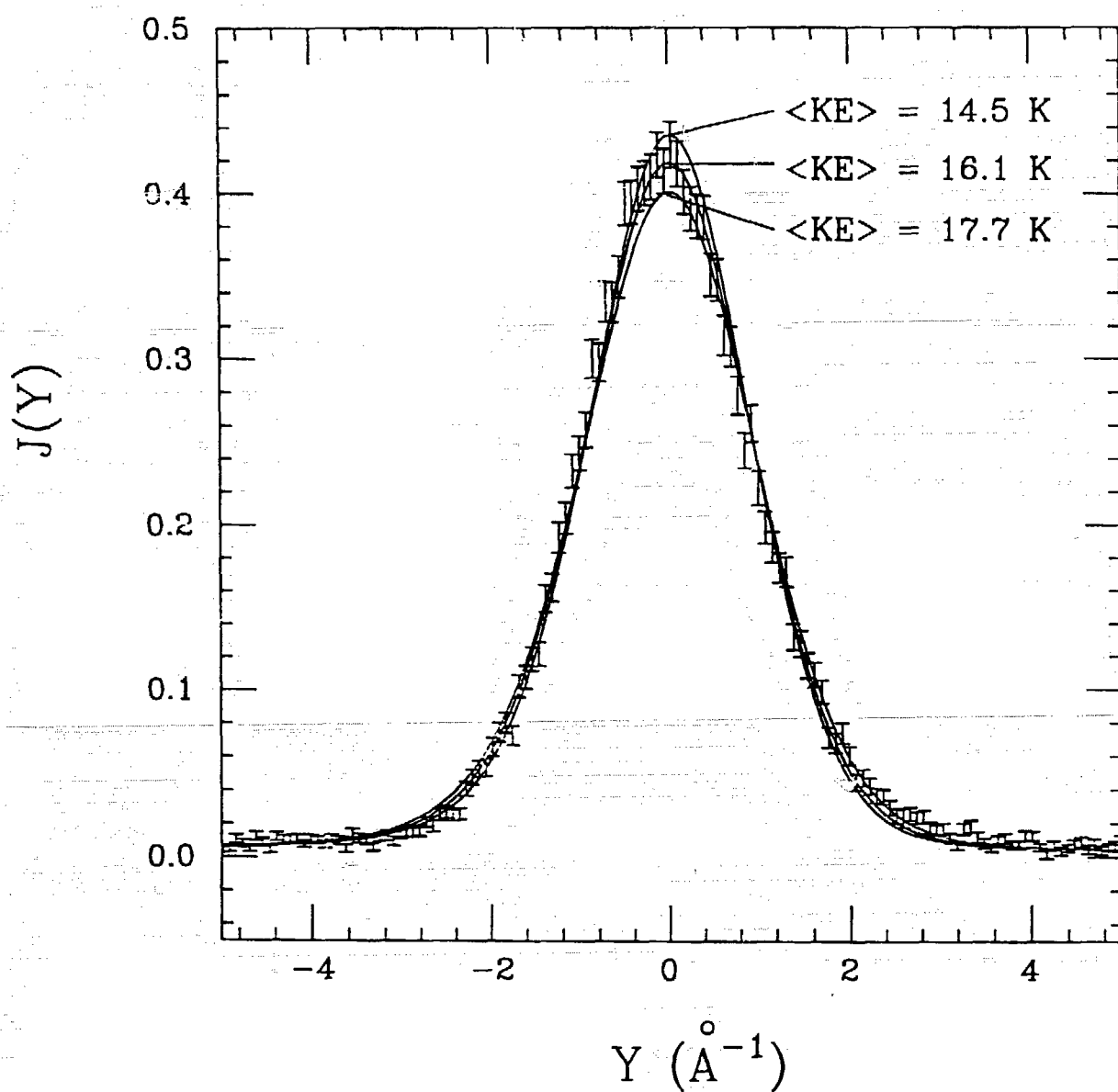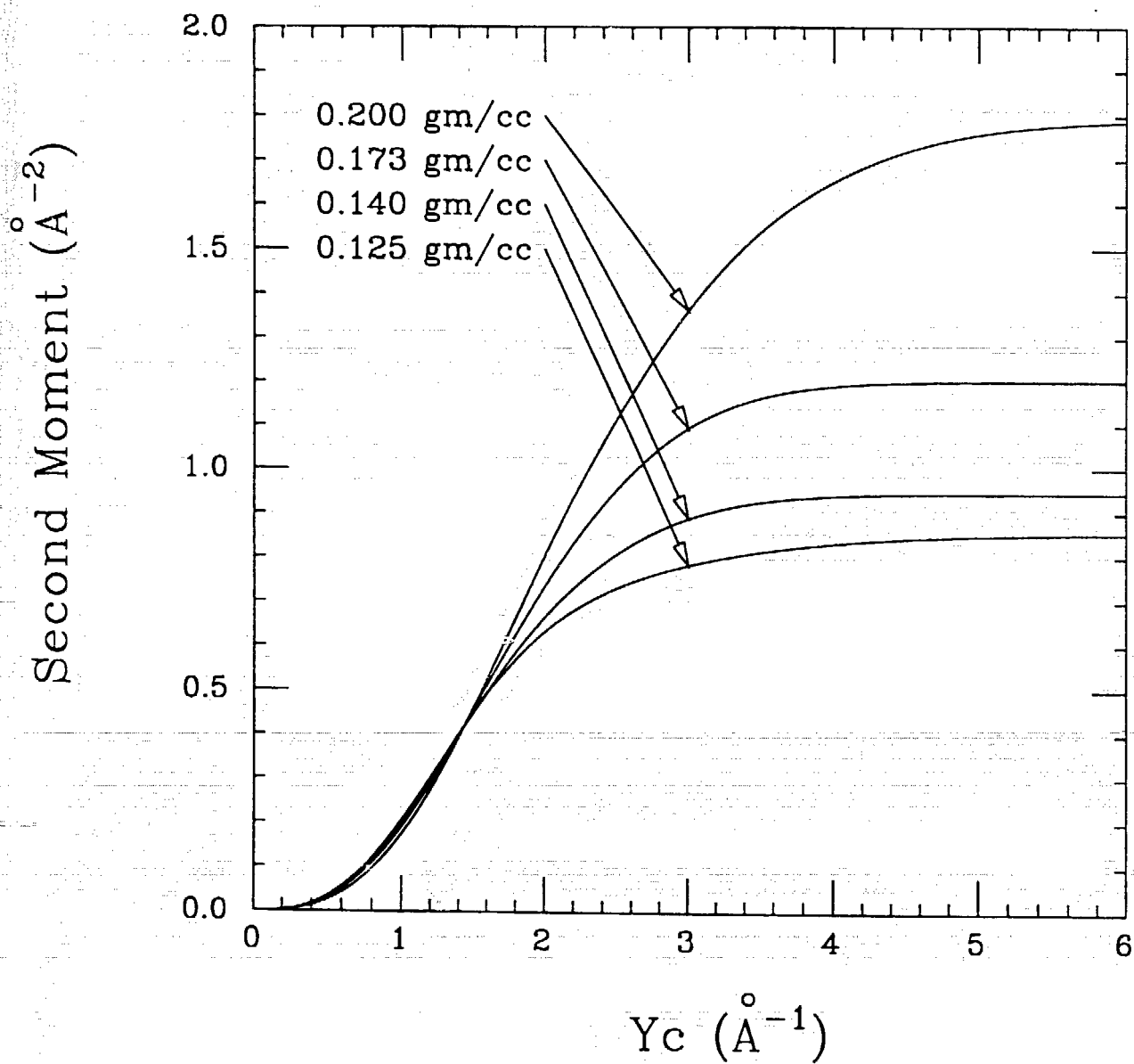Second Moment ($\overset{\circ}{A}{}^{-2}$)

Yc ($\overset{\circ}{A}{}^{-1}$)

$\langle KE \rangle = 14.5$ K

$\langle KE \rangle = 16.1$ K

$\langle KE \rangle = 17.7$ K

The figure shows a plot of Second Moment ($\mathring{A}^{-2}$) versus Y_c ($\mathring{A}^{-1}$) with curves labeled 0.200 gm/cc, 0.173 gm/cc, 0.140 gm/cc, and 0.125 gm/cc.